




Cadmium sulphide-sensitized zirconium dioxide (ZrO₂) photoanode by successive ionic layer adsorption and reaction for solar cell application

Bikram Prasad^{1,2}, Akanksha S. Chougale¹, Sandesh R. Jadkar¹, Nithesh Naik^{3,*} , and Habib M. Pathan^{1,*}

¹Advanced Physics Laboratory, Department of Physics, Savitribai Phule Pune University, Pune, Maharashtra 411007, India

²Department of Physics, Shri Mahanath Shatanand Giri College, Sherghati, Gaya, Bihar 824211, India

³Department of Mechanical and Industrial Engineering, Manipal Institute of Technology, Manipal Academy of Higher Education, Manipal, Karnataka 576104, India

Received: 20 August 2022

Accepted: 28 November 2022

Published online:

25 January 2023

© The Author(s) 2023

ABSTRACT

In the present study, cadmium sulphide (CdS) quantum dot-sensitized ZrO₂ photoanodes have been analysed by using the facial and cost-effective method, popularly known as successive ionic layer adsorption and reaction (SILAR), performed at 300 K. The presence of compact layer and ZnS treatment of the as-prepared photoanode is studied in this article to improve the solar cell parameters. The X-ray diffraction peaks infer the nano-crystalline nature of ZrO₂ films with an average particle size of 39.14 nm. The CdS-sensitized ZrO₂ films show a significant increase in absorption of photons in the visible region (i.e., 200 to 520 nm) of the absorption spectrum, as we have increased the number of SILAR cycles. Poly-sulphide electrolytes have been prepared in double distilled water and carbon black soot on conducting substrate is used as a counter electrode to be economical. The *J*-*V* characteristic of 10 CdS/ZrO₂ with a compact layer of TiO₂ with surface passivation (ZnS) treatment gives the maximum *J*_{sc} of 1.46 mA/cm² with a fill factor of 0.34 and conversion efficiency of 0.46%. Electrochemical impedance spectroscopy of the quantum dot-sensitized solar cell is studied to understand the kinetics of charge transfer and transport processes mechanisms involved.

1 Introduction

Researchers have conducted intensive and extensive research since the invention of the solar cell to harness clean solar energy due to the limited availability

of natural resources such as coal, petroleum, and natural gas on the planet [1]. The use of solar cells reduces the production of hazardous chemicals into the atmosphere and will help to meet current energy demand while also reducing carbon emissions [2].

Address correspondence to E-mail: nithesh.naik@manipal.edu; pathan@physics.unipune.ac.in

Researchers have looked at zirconia (ZrO_2) because of its exceptional physical, optical, and chemical qualities, such as possessing a high dielectric constant, a high melting point, chemical stability, low electrical conductivity, and biocompatibility [3–6]. According to the available literature, the reported band gap of ZrO_2 material is around 5.6–6.2 eV [7]. Three polymorphs of ZrO_2 exist and the phase change of zirconia takes place from monoclinic to tetragonal and to cubic as the temperature is increased, which leads to higher symmetry [3, 8, 9].

In the past few decades, group II–VI nano-crystalline semiconductors are intensively utilized for their highly distinctive features, which are not present in the bulk form. Nanoparticles have a very large surface-to-volume ratio [10] and one can synthesize these materials for specific study and application by regulating the particle size and shape by different ways of film deposition, which leads to a quantum size effect below a certain size [11, 12]. The bulk CdS particles are possessing a direct band gap of 2.42 eV [13]. The particles lower or equal to the Bohr excitonic radius give rise to a new form of system, known as quantum dots (QDs), which results in energy gap separation between the valence band and conduction band of the QDs [14].

QDs are nano-crystalline semiconductors having narrow band gaps like CdS, PbS, CdTe, CdSe, etc., and these have unique properties with respect to their bulk part making them more useful [15–19]. These properties include tuneable energy band gaps due to the quantum confinement effect, multiple exciton generation (MEG), and electronics, which help in improving efficiency and having higher absorption coefficients for different wavelengths in the solar spectrum [20–23]. The absorption mechanism of quantum dot-sensitized solar cells (QDSSC) is as follows: firstly, the incident photons excite the QDs valence band (VB) electrons to the conduction band (CB); secondly, these excited electrons are injected from the QD CB to the zirconia CB by the diffusion process and finally injected into the FTO and flow through an external circuit and simultaneously a redox electrolyte is regenerating the oxidized QDs by the acceptance of electron from the external circuit [24, 25]. The charge transfer mechanism in QDSSC is shown in Fig. 1.

Bare ZrO_2 porous films were sensitized with 0.02 molar concentration of CdS and 0.02 molar concentration of sodium sulphide, by the process known as

SILAR, which involves first dipping the deposited zirconia film (photoanode) into the cadmium precursor solution for 30 s, second rinsing it with double distilled water (DDW), third dipping the same electrode in the sulphur precursor solution to obtain CdS for 30 s, and fourth rinsing it with DDW. For the above-mentioned, the cadmium nitrate and sodium sulphide were dissolved in 25 ml of DDW. These four stages of dipping and rinsing the metal oxide film electrode are called one cycle of SILAR. The adsorbed concentration of CdS by this method on the ZrO_2 films can be further increased by reperforming the same cycle number of times [26].

Photovoltaic parameters of the solar cell like fill factor (FF), short circuit current density (J_{sc}), voltage due to open circuit (V_{oc}), input power (P_{in}), and the power conversion efficiency (η) are depicted in Table 1. The photovoltaic conversion efficiency of the as-prepared solar cell is calculated using Eq. (1),

$$\eta = \frac{FF V_{oc} J_{sc}}{P_{in}}. \quad (1)$$

In the present study, to minimize the recombination losses, the application of the compact blocking layer on the cleaned transparent conducting glass substrate is carried out that has a resistance of approximately 30 Ω and also given the ZnS treatment to passivate the surface of the photoanode, which reduces the recombination of the electrons at the different interfaces and also minimizes the surface trap states at the QDs/metal oxide interface [27, 28]. This also helps in reducing the band offsets and thereby increasing the diffusion of electrons from the conduction band of the sensitizer to the zirconia conduction band.

2 Experiments

The list of chemicals that were used in the present study for the process of deposition and sensitization of the photoanode with the preparation of the electrolyte and counter electrode are; ZrO_2 nanopowder (particle size approx. 45 nm) from SRL, ethyl cellulose from SDFCL, acetyl acetone from HPLC, terpineol from LC, sodium sulphide [Na_2S] from Sigma-Aldrich, sodium hydroxide [NaOH] from Sigma-Aldrich, sulphur powder from CDH, ethanol from CHFC, cadmium nitrate [$\text{Cd}(\text{NO}_3)_2$], titanium trichloride [TiCl_3] from LC, and zinc acetate

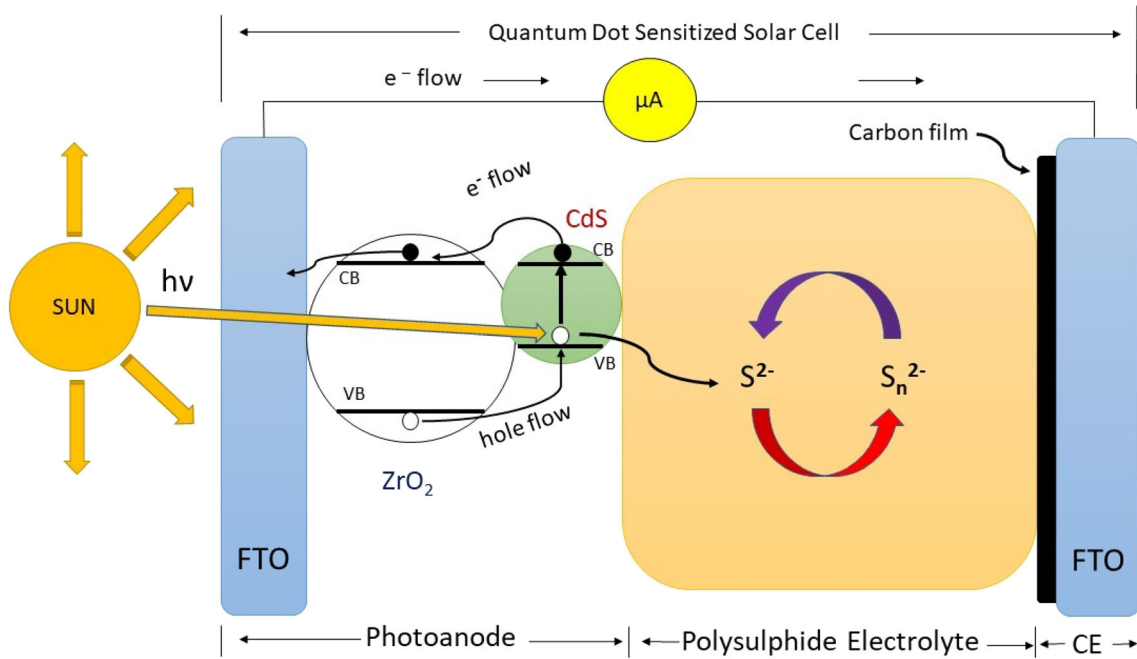


Fig. 1 Charge transfer mechanism of electrons and holes in QDSSC

Table 1 Elemental analysis of annealed ZrO₂ film with 05 CdS/ZrO₂, 10 CdS/ZrO₂, and 15 CdS/ZrO₂ films with the weight and atomic percentage of each element

S. no.	Sample name	Elements	wt%	at. %
1	Annealed ZrO ₂ film	Zr	63.76	16.34
		O	57.24	83.66
2	05 CdS/ZrO ₂ film	Cd	0.23	0.05
		S	0.14	0.10
		Zr	63.86	16.73
		O	55.63	83.12
3	10 CdS/ZrO ₂ film	Cd	2.54	0.54
		S	0.77	0.58
		Zr	65.53	17.25
		O	54.39	81.63
4	15 CdS/ZrO ₂ film	Cd	0.26	0.07
		S	0.14	0.12
		Zr	1.34	0.41
		O	56.43	99.40

[Zn(CH₃CO₂)₂] from SRL. These chemicals were utilized as received from the manufacturer.

2.1 Preparation method of zirconia paste and deposition of a film

0.25 g of ZrO₂ commercial nanopowder was ground with 5 ml of ethanol. A few grams of ethylcellulose

were taken and ground in a separate mortar pestle for 10 min and was mixed with an above-mentioned solution followed by ultrasonication. Further few millilitres of terpineol were added, which helps to reduce the surface tension of the paste and helps in coating the film evenly on the FTO surface. This mixture was ultrasonicated for 3 h and later 0.5 ml of Acetyl acetone was further added to the prepared solution and again ultrasonicated for 60 min to get the desired ZrO₂ paste. The extra ethanol was evaporated by keeping the paste in the incubator until we get a proper viscous paste of ZrO₂. This paste was prepared at 300 K.

The ZrO₂ paste was applied on the ultrasonicated cleaned substrate i.e., fluorine-doped tin oxide (FTO) by the method of doctor blading to have a uniform film of the required thickness which was followed by drying of the films in the incubator for 30 min at 60 °C. The spacer is provided with the help of scotch tape layers. Before placing the films in a hot furnace, they have been kept for a few hours in the incubator to get solidified by evaporating the extra ethanol. Now, these films were kept in a muffle furnace for annealing at 450 °C for 60 min in an oxygen environment. The films were allowed to cool inside the muffle furnace until the room temperature reached. The annealed film is a white-porous film with a granular morphology.

2.2 Sensitization of annealed ZrO₂ films using CdS by SILAR method

The CdS sensitization of annealed ZrO₂ films was done by SILAR, which helps in depositing the CdS QDs evenly on the metal oxide film. Here, the first beaker contains 10 mM of Cd(NO₃)₂ in 25 ml double distilled water (DDW), the second beaker contains 25 ml DDW, the third beaker contains 10 mM of Na₂S in 25 ml DDW, and the fourth beaker contains 25 ml DDW.

The photoelectrode was dipped in the first beaker for 30 s to get adsorb Cd²⁺ ions on the ZrO₂ photoelectrode due to electrostatic and Van der Waals forces and then rinsed for 30 s in the second beaker to detach loosely bounded Cd²⁺ ions, again dipped in the third beaker containing anionic precursor, namely sulphur (S²⁻), for 30 s to react with the Cd²⁺ ions resulting in the formation of CdS QDs and rinsed for 30 s in the fourth beaker to remove the excess anions. These steps comprise one SILAR cycle of CdS QDs on the photoelectrode to form CdS QD-sensitized photoanode. Likewise, 5, 10, and 15 cycles of SILAR were performed to load different amounts of CdS on the ZrO₂ films and as shown in Fig. 2.

2.3 Electrolyte preparation

The preparation of polysulphide electrolyte was done by taking 0.1 M of sodium sulphide in 25 ml DDW and grinding for 10 min. Now 0.4 g NaOH pellets were crushed and ground in a separate mortar pestle and later on 0.32 g of sulphur powder was added. Now the mortar pestle containing Na₂S was mixed with the NaOH and sulphur solution to form a polysulphide electrolyte, which is yellowish on account of sulphur presence. This electrolyte is considered to be highly efficient for QDSSCs applications [29, 30].

2.4 Counter electrode preparation

The FTO was ultrasonicated for 30 min and further washed with DDW and with the help of candle soot, a film of carbon black was coated and an area equal to 1 cm² was selected. The remaining region of the counter electrode which is not covered with carbon black provides the back contact.

The following instruments were used to record and draw the various data from the samples: UV-Visible

spectrophotometer (JASCO UV, V-770) having a wavelength range of 200–800 nm, X-ray diffractometer (XRD) (model: XRD, Rigaku “D/B max-2400”, Cu K_α with $\lambda = 1.54 \text{ \AA}$) and field emission scanning electron microscopy (FESEM) (Carl Zeiss, Merlin Compact), Potentiostat/Galvanostat (IVIUM Technologies Vertex model) and 2420 Keithley source meter [31].

3 Results and discussion

The X-ray diffraction peak graph of annealed zirconia film and CdS-sensitized films on ZrO₂ films for 5, 10, and 15 SILAR cycles is shown in Fig. 3. The peaks (011), (111), (200), and (220) present in the graph matches with the JCPDS card number 37-1484 and confirms that the deposited material is ZrO₂ and has monoclinic phase [32]. Similarly, the peaks (202), (203), (213), and (321) present matches with the JCPDS card number 02-0563 confirming the formation of the hexagonal phase of CdS material [33], and the peaks represented by F corresponds to the JCPDS card number 18-1387 which confirms the fluorine doped tin oxide (FTO) (SnO₂:F) material which was used as a substrate [34].

These intensity peaks confirm the coating of CdS over the ZrO₂ surface. The obtained crystallite size ranges from 40 to 55 nm, which was calculated by the Debye–Scherrer formula:

$$D = \frac{K\lambda}{\beta \cos \theta}. \quad (2)$$

[*D* is the crystallite size of the particle in nanometers, *K* is the geometry factor of the prepared material (0.89 for the prepared spherical particles of ZrO₂), λ is 1.54 Å (incident X-ray wavelength), β is the full-width half maxima in radians, and θ is the Bragg’s angle in degrees]

The UV–visible spectroscopy of these as-prepared films was taken and studied for absorption and band gap determination and is shown in Fig. 4.

As per Fig. 4a, the UV–Visible absorption spectroscopy of the as-prepared films clearly shows the absorption of light by the CdS-loaded films increases with the increase of the number of SILAR cycles of CdS. The 15 CdS/ZrO₂ film shows the maximum absorption of the incident light in the UV to a visible wavelength range from 200 to 700 nm, whereas Fig. 4b is the energy (eV) versus the square of the

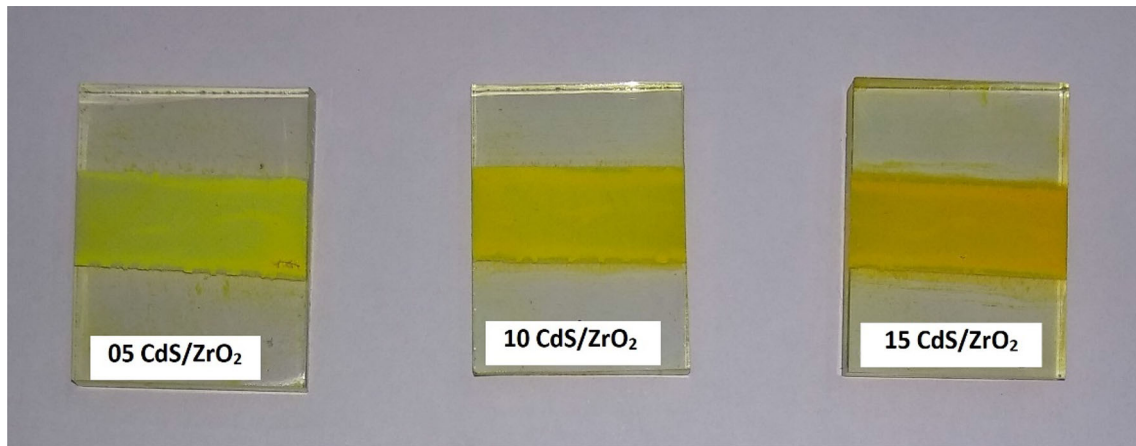
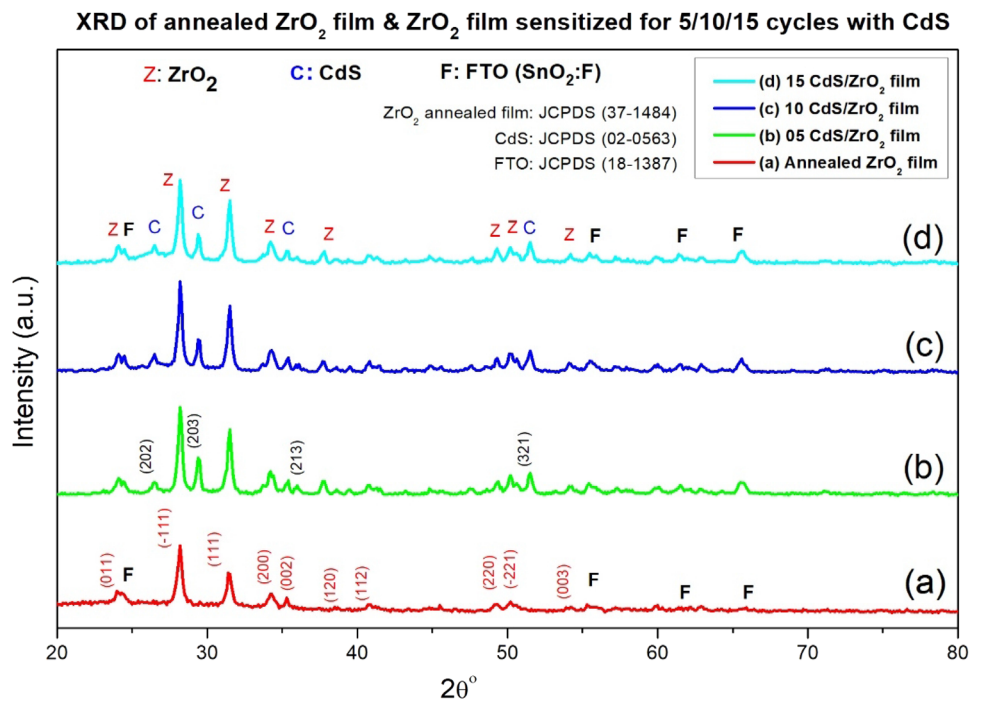


Fig. 2 As-prepared CdS-sensitized ZrO₂ films with 05, 10, and 15 SILAR cycles

Fig. 3 X-ray diffraction peak pattern of **a** Annealed ZrO₂ film, **b** 05 CdS/ZrO₂ film, **c** 10 CdS/ZrO₂ film, **d** 15 CdS/ZrO₂ film



absorbance plot of the as-prepared films. The calculated energy band gap of the annealed ZrO₂ film, 05 CdS/ZrO₂ film, 10 CdS/ZrO₂ film, and 15 CdS/ZrO₂ film are 5.15 eV, 3.55 eV, 2.46 eV, and 2.40 eV, respectively. The optical absorption spectra show, there is a redshift, i.e., decreasing optical band gap with the increase in SILAR cycles of CdS. In 15 CdS/ZrO₂ the aggregation of CdS over ZrO₂ results in the formation of bigger particles of CdS at the expense of smaller CdS nanoparticles and thereby decreasing the optical band gap, which is the inherent property of bulk particles.

The surface morphology of the as-prepared films was studied by using FESEM, which shows the porous morphology of the annealed ZrO₂ film and the subsequent images confirms the uniform coating of CdS particles over the porous ZrO₂ film. Granular and Porous morphology is seen after annealing the film and the whitish part seen in the images is CdS adsorbed layer on ZrO₂ film after the adsorption of CdS through SILAR. In Fig. 5, one can see that there is an aggregation of CdS particles on the surface of ZrO₂ film for higher SILAR cycles.

The EDS graph from Fig. 6 shows the corresponding elemental peaks for the present elements in

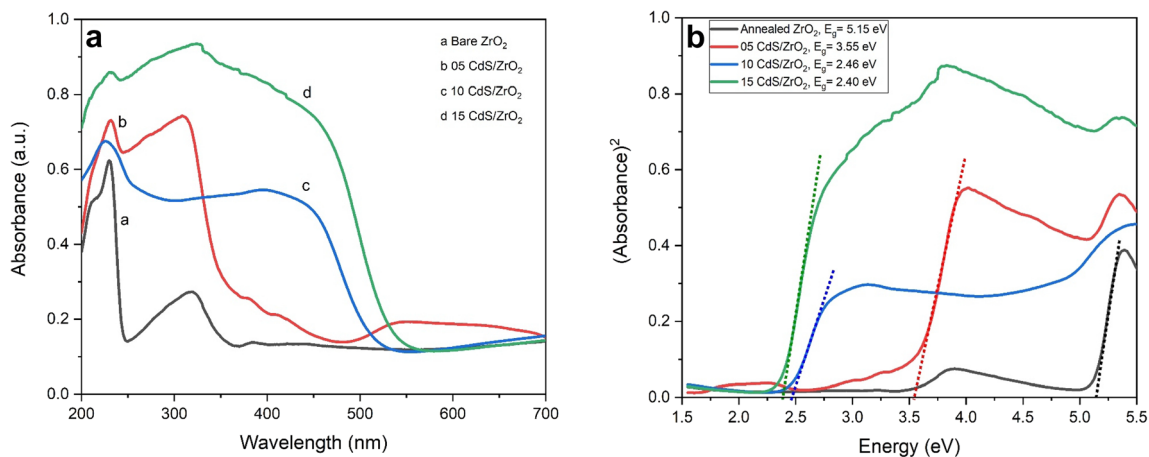


Fig. 4 UV-visible absorption spectra for **a** the as-prepared films and **b** the Square of absorbance versus Energy (eV)

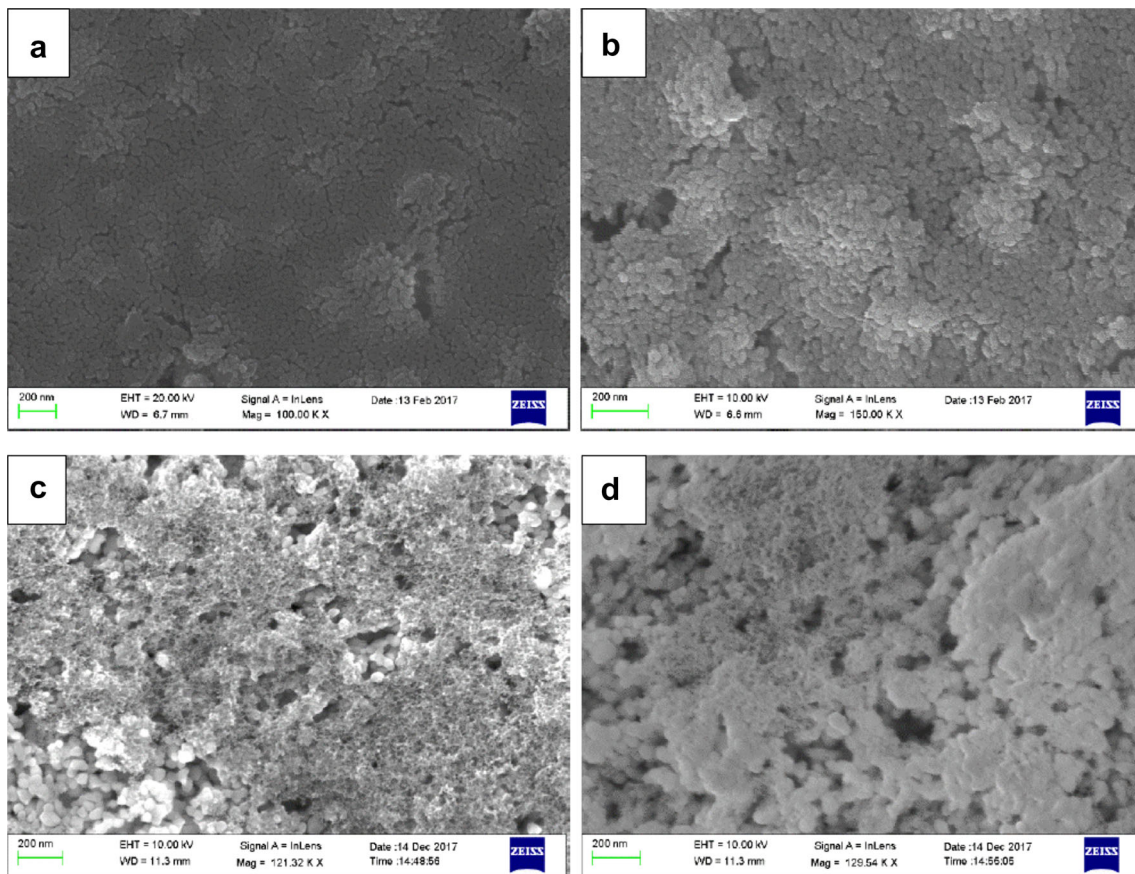


Fig. 5 FESEM image of **a** Annealed ZrO_2 film, **b** 05 CdS/ZrO_2 film, **c** 10 CdS/ZrO_2 film, **d** 15 CdS/ZrO_2 film

the film with respect to the incident energy. This graph also shows the contamination present if any [8]. The table shows the proportion of elements present in the synthesized film in atomic percentage. Table 1 suggests that a good amount of CdS has been

loaded on the 10 CdS/ZrO_2 film. From Table 1, it can be seen that there is 16.34 at.% of Zr and 83.66 at.% of O in the EDS, which confirms the presence of ZrO_2 (Fig. 7).

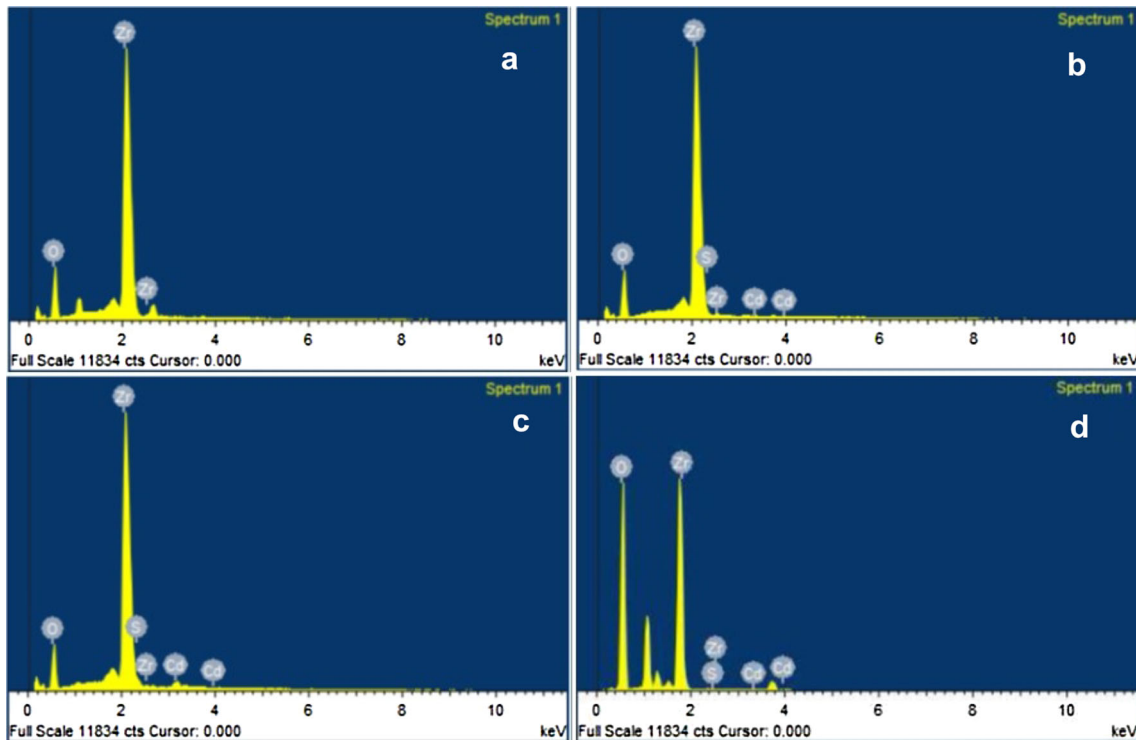


Fig. 6 EDS of a ZrO₂ film, b 0.5 CdS/ZrO₂ film, c 1.0 CdS/ZrO₂ film, d 1.5 CdS/ZrO₂ film

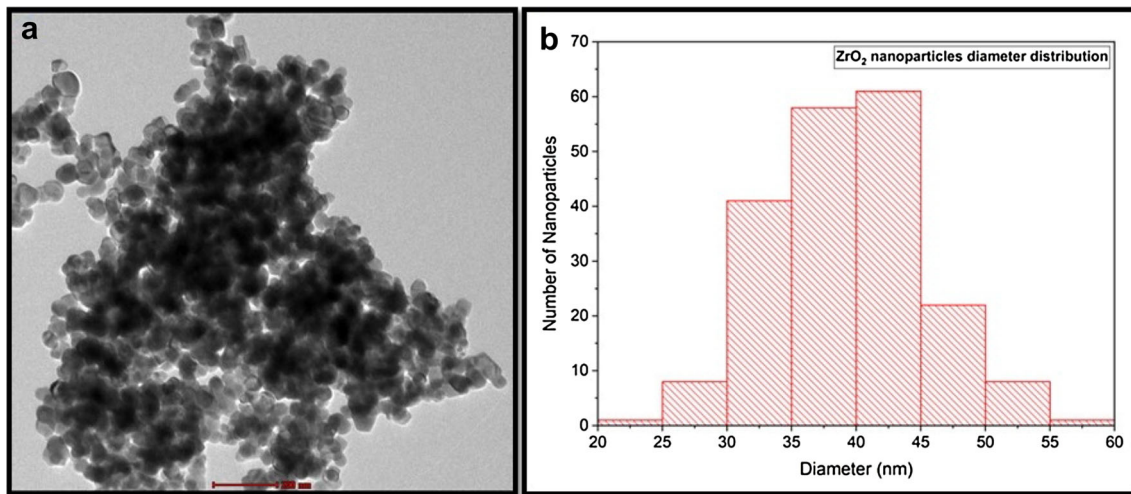


Fig. 7 a TEM of ZrO₂ nanoparticles, b ZrO₂ nanoparticles diameter distribution

The ZrO₂ nanoparticle diameters were found in between the 20 and 60 nm range with an average nanoparticle diameter of size 39.14 nm. The number of ZrO₂ nanoparticles samples taken to find the average nanoparticle diameter is 200. The diameter data are collected by using Image J software and plotted the histogram to find the average diameter of ZrO₂ nanoparticles and by using the Gaussian distribution function in the same software.

Table 2 shows CdS/ZrO₂ films without a compact layer exhibit negligible efficiency and poor fill factor due to cell shorting (i.e., pinholes present in the as-prepared ZrO₂ layer), which means excited electrons directly find the path to move from the sensitizers conduction band to the FTO conduction band. As a result, photogenerated electron recombination losses occur. As a result, we must apply a compact layer to reduce these losses and create a pathway for excited

Table 2 Solar cell parameters with the standard structure of FTO/ZrO₂/CdS/polysulphide electrolyte/carbon black counter electrode with the number of SILAR cycles of CdS on ZrO₂ film, with compact layer and after ZnS treatment are shown below

Without CL	J_{sc} (mA/cm ²)	V_{oc} (mV)	FF	η (%)
Bare ZrO ₂	0.23	281	0.14	0.01
5 CdS/ZrO ₂	0.25	273	0.15	0.02
10 CdS/ZrO ₂	0.23	355	0.19	0.03
15 CdS/ZrO ₂	0.15	361	0.25	0.02
With CL	J_{sc} (mA/cm ²)	V_{oc} (mV)	FF	η (%)
5 CdS/ZrO ₂	0.67	547	0.30	0.19
10 CdS/ZrO ₂	0.99	618	0.44	0.45
15 CdS/ZrO ₂	1.46	680	0.37	0.60
With CL and ZnS Treatment	J_{sc} (mA/cm ²)	V_{oc} (mV)	FF	η (%)
5 CdS/ZrO ₂	1.28	619	0.29	0.33
10 CdS/ZrO ₂	1.46	563	0.34	0.46
15 CdS/ZrO ₂	1.06	557	0.27	0.27

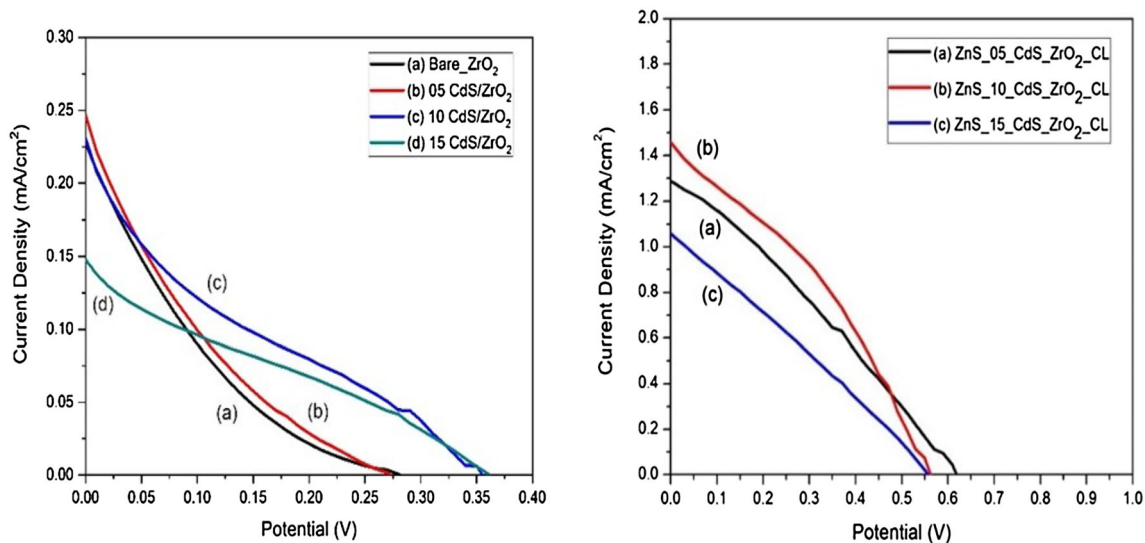
**Fig. 8** J - V curves for (i) ZrO₂ film and CdS/ZrO₂ films, and (ii) CdS/ZrO₂ films with CL and ZnS treatment

photo-electrons to travel smoothly from the sensitizer conduction band to the metal oxide conduction band and then to the FTO conduction band.

The bare ZrO₂ film and CdS-sensitized ZrO₂ photoanodes were tested in combination with carbon black as a counter electrode and poly-sulphide as an electrolyte with a mask of area 0.25 cm². As per Table 2, The 10 SILAR cycles of CdS-sensitized ZrO₂ film show better performance than 05 SILAR due to better fill factor and uniform loading of CdS on the ZrO₂ film. In 05 SILAR, there is lesser loading of CdS particles on ZrO₂, which results in a lesser area for

exciton generation, thereby low efficiency [35]. The lowering of current on the 15 CdS/ZrO₂ photoanodes is due to the agglomeration effect of CdS on the surface of ZrO₂ film during the SILAR cycles. These oversized nanoparticles can act as a potential barrier to the efficient charge transfer mechanism [36]. The stated J - V curves of CdS with ZrO₂ film are shown in Fig. 8. The maximum V_{oc} and J_{sc} for the 10 CdS/ZrO₂ solar cell are 355 mV and 0.23 mA cm⁻², respectively, observed.

To improve the solar cell parameters, TiO₂ compact layer has been applied. The cells having a compact layer

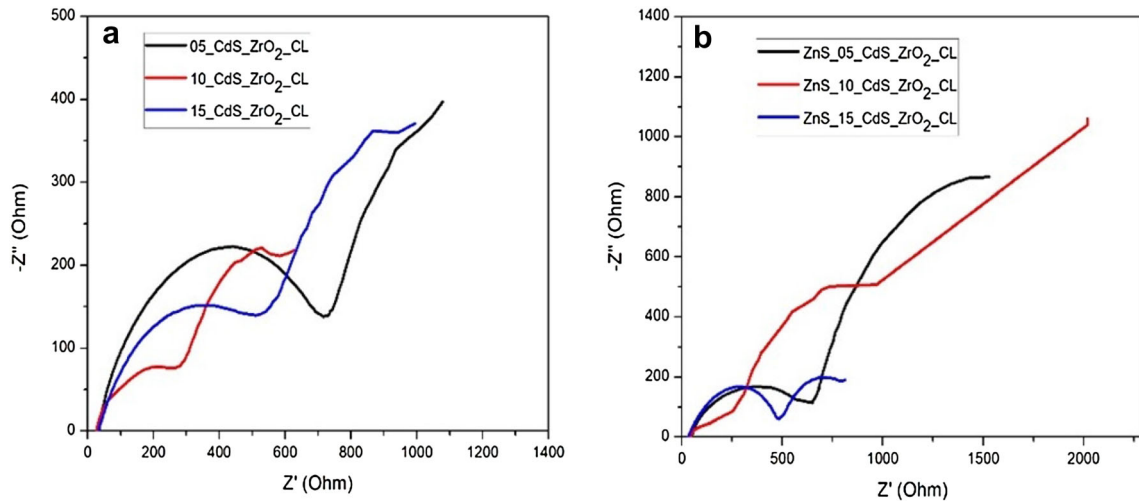


Fig. 9 Nyquist plot for a CdS/ZrO₂ films, and b CdS/ZrO₂ films with CL and ZnS treatment

Table 3 Photovoltaic performance of sensitized ZrO₂ photoelectrodes

S. no.	Sensitizers	J_{sc} (mA/cm ²)	V_{oc} (mV)	FF	η (%)	P_{in} (mW/cm ²)	Ref. No.
1	CdS type-a	0.89	770	0.30	0.68	30	[38]
2	CdS type-b	1.44	610	0.34	1.00	30	[38]
3	CdS type-c	1.78	440	0.24	0.62	30	[38]
4	CdS	1.46	563	0.34	0.46	60	Present study

between the FTO and metal oxide layer show a much better fill factor value than the one which does not have a compact layer. This layer helps in reducing the recombination losses. The lower value of the fill factor is seen due to the recombination loss of the electrons between the photoanode and the electrolyte. The value of the current is low due to the poor offset between the conduction band of both sensitizer and the photoanode [37]. As a result, ZnS treatment is applied to the ZrO₂ photoanode and was tested again under the same environment, which shows almost double the previous performance. ZnS treatment of the as-prepared cells gives better photocurrent by suppressing the recombination losses at various interfaces. To have a better fill factor, the device must have high recombination resistances and proper offset of the conduction band of the photoanode and the sensitizer. Even after surface passivation at 15/CdS/ZrO₂/CL, there is less value of current density (1.06 mA/cm²) due to aggregation of CdS on the zirconia film, whereas in 10/CdS/ZrO₂/CL after surface passivation we get the maximum value of current density (1.46 mA/cm²) with a fill factor of 0.34 and with a highest photon conversion efficiency of 0.46%.

Figure 9a shows the electrochemical impedance spectroscopy (EIS) of the as-prepared CdS/ZrO₂/CL for 5, 10, and 15 SILAR cycles, and the EIS for the as-prepared CdS/ZrO₂/CL with ZnS surface passivation treatment is shown in Fig. 9b. The abscissa, from 0 to 30 ohms, represents the resistance of FTO on which metal oxide is deposited. Here, the first semicircle shows the charge transfer resistance at the interface of the polysulphide electrolyte/carbon counter electrode [31]. The consecutive second semicircle shows the resistance at the CdS/ZrO₂ interface, yielding less fill factor and thereby we get an appreciable fill factor for 10/CdS/ZrO₂/CL photoanode. The complex chemistry of scavenging property of sulphur at electrolyte and carbon-coated counter electrode results in the overall degrading of the parameters of the solar cell. As a result, we need to place a compact layer and also need to reduce the recombination losses of the photoelectrons.

The extensive literature survey carried out shows only one research report available on CdS-sensitized ZrO₂ photoelectrodes. Table 3, shows the comparison of the photovoltaic performance performed by the Ravi et al. group to sensitized ZrO₂ photoelectrodes mentioned below with the photovoltaic parameters [38].

These reported cells show a higher value of J_{sc} , V_{oc} , FF, and efficiency due to low input power of 30 mW/cm², when compared to our result which was recorded at 60 mW/cm². Hence, as per Eq. (1), we can infer that a low value of input power will yield higher efficiency and vice versa. This suggests that our results in terms of efficiency are comparable to the reported CdS type-b for ZrO₂ solar cell applications.

4 Conclusion

The presence of the monoclinic phase of ZrO₂ as well as the hexagonal phase of CdS is confirmed by XRD analysis of the as-prepared CdS-based zirconia films. The porous morphology of the as-prepared zirconia film is revealed by FESEM images, which confirm the homogeneous adsorption of the CdS sensitizers on the zirconia film using the simple SILAR approach. Due to the optimal loading of CdS nanoparticles, the 10 CdS/ZrO₂ photoanode as a photovoltaic cell outperforms the 05 and 15 CdS/ZrO₂ photoanode cells on the J - V curve. The surface passivation of the photoanode helps to reduce the recombination losses of the photoelectrons in the cell.

Acknowledgements

The authors are very thankful to M. Priyanka, Prashant K. Baviskar, Chaitali Jagtap, Vishal S. Kadam, Snehal S. Wagh, Mangesh A. Waghmare, Ravi V. Ingle, and Niyamat I. Beedri for their fruitful discussion.

Author contributions

All authors contributed to the study conception and design. Material preparation, data collection, and analysis were performed by BP, ASC, SRJ, NN, and HMP. The first draft of the manuscript was written by BP, ASC and all authors commented on previous versions of the manuscript. All authors read and approved the final manuscript.

Funding

Open access funding provided by Manipal Academy of Higher Education, Manipal. The authors declare

that no funds, grants, or other support were received during the preparation of this manuscript.

Data availability

The data support of current findings is available from the corresponding author upon reasonable request.

Declarations

Competing interest The authors have no relevant financial or non-financial interests to disclose.

Open Access This article is licensed under a Creative Commons Attribution 4.0 International License, which permits use, sharing, adaptation, distribution and reproduction in any medium or format, as long as you give appropriate credit to the original author(s) and the source, provide a link to the Creative Commons licence, and indicate if changes were made. The images or other third party material in this article are included in the article's Creative Commons licence, unless indicated otherwise in a credit line to the material. If material is not included in the article's Creative Commons licence and your intended use is not permitted by statutory regulation or exceeds the permitted use, you will need to obtain permission directly from the copyright holder. To view a copy of this licence, visit <http://creativecommons.org/licenses/by/4.0/>.

References

1. Z. Pan, H. Rao, I. Mora-Seró, J. Bisquert, X. Zhong, Quantum dot-sensitized solar cells. *Chem. Soc. Rev.* **47**(20), 7659–7702 (2018). <https://doi.org/10.1039/c8cs00431e>
2. M.Z. Jacobson, M.A. Delucchi, Providing all global energy with wind, water, and solar power, part I: technologies, energy resources, quantities and areas of infrastructure, and materials. *Energy Policy* (2011). <https://doi.org/10.1016/j.enpol.2010.11.040>
3. M.A. Waghmare, M. Naushad, Z.A. Allothman, A.U. Ubale, H.M. Pathan, Zirconium oxide films: deposition techniques and their applications in dye-sensitized solar cells. *J. Solid State Electrochem.* (2017). <https://doi.org/10.1007/s10008-017-3565-8>
4. K. Khojier, H. Savaloni, F. Jafari, Structural, electrical, and decorative properties of sputtered zirconium thin films during

- post-annealing process. *J. Theor. Appl. Phys.* (2013). <https://doi.org/10.1186/2251-7235-7-55>
5. K. Joy, I.J. Berlin, P.B. Nair, J.S. Lakshmi, G.P. Daniel, P.V. Thomas, Effects of annealing temperature on the structural and photoluminescence properties of nanocrystalline ZrO₂ thin films prepared by sol–gel route. *J. Phys. Chem. Solids* (2011). <https://doi.org/10.1016/j.jpcs.2011.02.012>
 6. W. Li, X. Liu, A. Huang, P.K. Chu, Structure and properties of zirconia (ZrO₂) films fabricated by plasma-assisted cathodic arc deposition. *J. Phys. D Appl. Phys.* (2007). <https://doi.org/10.1088/0022-3727/40/8/S08>
 7. H. Nohira et al., Characterization of ALCVD-Al₂O₃ and ZrO₂ layer using X-ray photoelectron spectroscopy. *J. Non Cryst. Solids* (2002). [https://doi.org/10.1016/S0022-3093\(02\)00970-5](https://doi.org/10.1016/S0022-3093(02)00970-5)
 8. M.A. Waghmare, M. Naushad, H.M. Pathan, A.U. Ubale, Rose bengal-sensitized ZrO₂ photoanode for dye-sensitized solar cell. *J. Solid State Electrochem.* **21**(9), 2719–2723 (2017). <https://doi.org/10.1007/s10008-017-3530-6>
 9. S.M. Chang, R.A. Doong, Interband transitions in sol-gel-derived ZrO₂ films under different calcination conditions. *Chem. Mater.* **19**, 4804–4810 (2007). <https://doi.org/10.1021/cm070606n>
 10. M.B. Rajendra Prasad, H.M. Pathan, Effect of photoanode surface coverage by a sensitizer on the photovoltaic performance of titania based CdS quantum dot sensitized solar cells. *Nanotechnology* (2016). <https://doi.org/10.1088/0957-4484/27/14/145402>
 11. R. Elilarassi, S. Maheshwari, G. Chandrasekaran, Structural and optical characterization of CdS nanoparticles synthesized using a simple chemical reaction route. *Optoelectron. Adv. Mater. Rapid Commun.* **4**(3), 309–312 (2010)
 12. W.W. Yu, L. Qu, W. Guo, X. Peng, Experimental determination of the extinction coefficient of CdTe, CdSe, and CdS nanocrystals. *Chem. Mater.* **125**(17), 2854–2860 (2003)
 13. N. Qutub, S. Sabir, Optical, thermal and structural properties of CdS quantum dots synthesized by a simple chemical route. *Int. J. Nanosci. Nanotechnol.* **8**(2), 111–120 (2012)
 14. S.M. Abed, S. Naif, T. Al, Study of effect the particle size on CdS optical properties as solar cell. *AUS* (2019). <https://doi.org/10.4206/aus.2019.n26.2.6>
 15. Y.J. Shen, Y.L. Lee, Assembly of CdS quantum dots onto mesoscopic TiO₂ films for quantum dot-sensitized solar cell applications. *Nanotechnology* (2008). <https://doi.org/10.1088/0957-4484/19/04/045602>
 16. M.N. Borovaya, A.P. Naumenko, N.A. Matvieieva, Y.B. Blume, A.I. Yemets, Biosynthesis of luminescent CdS quantum dots using plant hairy root culture. *Nanoscale Res. Lett.* **9**(1), 1–7 (2014). <https://doi.org/10.1186/1556-276X-9-686>
 17. T. Ha Thanh, D. Huynh Thanh, V. Quang Lam, The CdS/CdSe/ZnS photoanode cosensitized solar cells based on Pt, CuS, Cu₂S, and PbS counter electrodes. *Adv. Optoelectron.* (2014). <https://doi.org/10.1155/2014/397681>
 18. G. Liu, S. Ji, G. Xu, C. Ye, Interface engineering: boosting the energy conversion efficiencies for nanostructured solar cells. *Pure Appl. Chem.* **84**(12), 2653–2675 (2012). <https://doi.org/10.1351/PAC-CON-11-11-05>
 19. C.H. Chang, Y.L. Lee, Chemical bath deposition of CdS quantum dots onto mesoscopic TiO₂ films for application in quantum-dot-sensitized solar cells. *Appl. Phys. Lett.* **91**(5), 2–5 (2007). <https://doi.org/10.1063/1.2768311>
 20. T. Ahamad, M.A. Majeed Khan, S. Kumar, M. Ahamed, M. Shahabuddin, A.N. Alhazaa, CdS quantum dots: growth, microstructural, optical and electrical characteristics. *Appl. Phys. B Lasers Opt.* **122**(6), 1–8 (2016). <https://doi.org/10.1007/s00340-016-6455-3>
 21. S. Greenwald, S. Rühle, M. Shalom, S. Yahav, A. Zaban, Unpredicted electron injection in CdS/CdSe quantum dot sensitized ZrO₂ solar cells. *Phys. Chem. Chem. Phys.* (2011). <https://doi.org/10.1039/c1cp22290b>
 22. P. Devendran, T. Alagesan, T.R. Ravindran, K. Pandian, Synthesis of spherical CdS quantum dots using cadmium diethyldithiocarbamate as single source precursor in olive oil medium. *Curr. Nanosci.* **10**(2), 302–307 (2014). <https://doi.org/10.2174/15734137113096660117>
 23. Y. Wang, N. Herron, Nanometer-sized semiconductor clusters: materials synthesis, quantum size effects, and photo-physical properties. *J. Phys. Chem.* **95**(2), 525–532 (1991). <https://doi.org/10.1021/j100155a009>
 24. I. Hod, A. Zaban, Materials and interfaces in quantum dot sensitized solar cells: challenges, advances and prospects. *Langmuir* (2014). <https://doi.org/10.1021/la403768j>
 25. J. Duan, H. Zhang, Q. Tang, B. He, L. Yu, Recent advances in critical materials for quantum dot-sensitized solar cells: a review. *J. Mater. Chem. A* (2015). <https://doi.org/10.1039/c5ta03280f>
 26. C.-H. Chang, Y.-L. Lee, Chemical bath deposition of CdS quantum dots onto mesoscopic TiO₂ films for application in quantum-dot-sensitized solar cells. *Appl. Phys. Lett.* **10**(1063/1), 2768311 (2007)
 27. S. Giménez et al., Improving the performance of colloidal quantum-dot-sensitized solar cells. *Nanotechnology* (2009). <https://doi.org/10.1088/0957-4484/20/29/295204>
 28. N.T.K. Chung, P.T. Nguyen, H.T. Tung, D.H. Phuc, Quantum dot sensitized solar cell: photoanodes, counter electrodes, and electrolytes. *Molecules* (2021). <https://doi.org/10.3390/molecules26092638>
 29. Y.L. Lee, C.H. Chang, Efficient polysulfide electrolyte for CdS quantum dot-sensitized solar cells. *J. Power Sources*

- 185(1), 584–588 (2008). <https://doi.org/10.1016/j.jpowsour.2008.07.014>
30. L. Li et al., Highly efficient CdS quantum dot-sensitized solar cells based on a modified polysulfide electrolyte. *J. Am. Chem. Soc.* **133**(22), 8458–8460 (2011). <https://doi.org/10.1021/ja201841p>
31. V.P. Bhalekar, P.K. Baviskar, B. Prasad, N.I. Beedri, V.S. Kadam, H.M. Pathan, Lead sulphide sensitized ZrO₂ photoanode for solar cell application with MoO₃ as a counter electrode. *Chem. Phys. Lett.* (2017). <https://doi.org/10.1016/j.cplett.2017.10.001>
32. W. Cao, J. Kang, G. Fan, L. Yang, F. Li, Fabrication of porous ZrO₂ nanostructures with controlled crystalline phases and structures via a facile and cost-effective hydrothermal approach. *Ind. Eng. Chem. Res.* **54**(51), 12795–12804 (2015). <https://doi.org/10.1021/acs.iecr.5b03114>
33. S.N. Basahel, T.T. Ali, M. Mokhtar, K. Narasimharao, Influence of crystal structure of nanosized ZrO₂ on photocatalytic degradation of methyl orange. *Nanoscale Res. Lett.* (2015). <https://doi.org/10.1186/s11671-015-0780-z>
34. S. Thirumavalavan, D. Mohan Venkat, G. Mohan Kumar, D. Srikanth, Synthesis and characterization of cadmium sulfide nano particles. *Int. J. Recent Technol. Eng.* **7**(6), 649–652 (2019)
35. H.J. Lee et al., Regenerative PbS and CdS quantum dot sensitized solar cells with a cobalt complex as hole mediator. *Langmuir* **25**(13), 7602–7608 (2009). <https://doi.org/10.1021/la900247r>
36. P. Lv et al., Photoelectrochemical property of CdS and PbS cosensitized on the TiO₂ array by novel successive ionic layer adsorption and reaction method. *J. Alloys Compd.* **621**, 30–34 (2015). <https://doi.org/10.1016/j.jallcom.2014.09.172>
37. C.F. Chi et al., Energy level alignment, electron injection, and charge recombination characteristics in CdS/CdSe cosensitized TiO₂ photoelectrode. *Appl. Phys. Lett.* **98**(1), 96–99 (2011). <https://doi.org/10.1063/1.3533642>
38. R.V. Ingle, A.T. Supekar, V.P. Bhalekar, B. Prasad, H.M. Pathan, The influence of polysulfide solvent on the performance of cadmium sulfide sensitized zirconium dioxide-based quantum dots. *ES Mater. Manuf.* **9**, 12–20 (2020). <https://doi.org/10.30919/esmm5f790>

Publisher's Note Springer Nature remains neutral with regard to jurisdictional claims in published maps and institutional affiliations.